J. Micromech. Microeng. **19** (2009) 074011 (10pp) doi:10.1088/0960-1317/19/7/074011

Catheter-based flexible microcoil RF detectors for internal magnetic resonance imaging

M M Ahmad[1], R R A Syms[1,4], I R Young[1], B Mathew[1], W Casperz[2], S D Taylor-Robinson[3], C A Wadsworth[3] and W M W Gedroyc[2]

[1] Optical and Semiconductor Devices Group, EEE Dept., Imperial College London, Exhibition Road, London SW7 2AZ, UK
[2] Department of Radiology, Imperial College NHS Trust, Praed St., Paddington, London W2 1NY, UK
[3] Department of Hepatology, Division of Medicine, Faculty of Medicine, Imperial College London, London W2 1PG, UK

E-mail: r.syms@imperial.ac.uk

Received 15 November 2008, in final form 4 February 2009
Published 30 June 2009
Online at stacks.iop.org/JMM/19/074011

Abstract
Flexible catheter probes for magnetic resonance imaging (MRI) of the bile duct are demonstrated. The probes consist of a cytology brush modified to accept a resonant RF detector based on a spiral microcoil and hybrid integrated capacitors, and are designed for insertion into the duct via a non-magnetic endoscope during endoscopic retrograde cholangiopancreatography (ERCP). The coil must be narrow enough (<3 mm) to pass through the biopsy channel of the endoscope and sufficiently flexible to turn through 90° to enter the duct. Coils are fabricated as multi-turn electroplated conductors on a flexible base, and two designs formed on SU-8 and polyimide substrates are compared. It is shown that careful control of thermal load is used to obtain useable mechanical properties from SU-8, and that polyimide/SU-8 composites offer improved mechanical reliability. Good electrical performance is demonstrated and sub-millimetre resolution is obtained in ^{1}H MRI experiments at 1.5 T magnetic field strength using test phantoms and *in vitro* liver tissue.

1. Introduction

Cholangiocarcinomas are malignant tumours of the lining of the bile duct that often evade detection until late, untreatable stages [1]. The bile duct supplies bile salts and bile acids secreted in the liver and temporarily stored in the gall bladder to the duodenum as shown in figure 1, to emulsify fats during digestion. The cause of the rising incidence of cholangiocarcinoma is unknown, but it may be due to agricultural chemical residuals or cirrhosis [2]. The tumours are generally insensitive to chemotherapy and radiotherapy, and only small (≈1 mm) tumours are operable with satisfactory outcome.

Imaging of the bile duct is currently performed during endoscopic retrograde cholangiopancreatography (ERCP) using fluoroscopic x-ray screening and a side-viewing flexible endoscope [3]. Direct viewing of the duct using the endoscope is only possible near its distal end, although catheter tools can be inserted via a side-opening biopsy channel as shown in figure 2(*a*). Histological confirmation involves sampling suspect regions with a cytology brush [4]. However, this process has a low-pickup rate, and potentially seeds cells along the duct. Clinicians also examine whole body image data using contrast-enhanced x-ray studies or magnetic resonance imaging (MRI). If a cholangiocarcinoma is present, it will be where the duct appears partly narrowed. MRI has sufficient contrast, but the sensitivity and resolution of hepatic MRI with external coils is insufficient to find 1 mm lesions reliably. One solution would be to introduce internal coils into the duct via a side-opening duodenoscope. Even greater advantage would follow from the ability to determine the origin of any sampled malignant cells, by combining an imaging probe with a cytology brush.

[4] Author to whom any correspondence should be addressed.

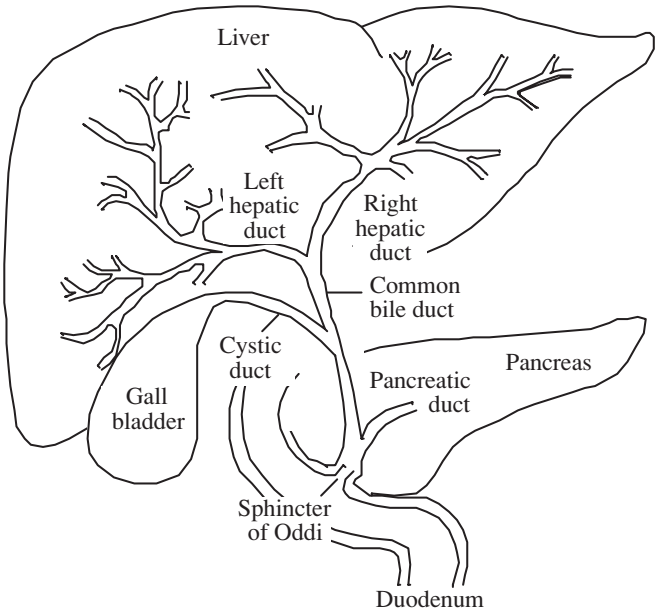

Figure 1. The biliary tree.

Catheter MR probes based on planar-loop, opposed-solenoid and twisted-pair coils have been developed for vascular imaging [5–8] and catheter tracking [9–12]. Intrabiliary imaging [13] has also been demonstrated using percutaneously inserted 'loopless catheter antennae' (which detect electric rather than magnetic fields) [14]. The detectors have generally been handmade, and there are clear advantages in size, reproducibility and cost in using batch fabrication processes. This approach would allow closely spaced multiturn planar coils to be integrated in a compact catheter that may be sent for histology or disposal after use.

Planar microcoils have been demonstrated on gallium arsenide [15, 16], silicon [17–19] and glass [20, 21]. However, most demonstrations have been confined to the laboratory and interest is now increasing in the use of plastic substrates such as polyimide, which offer good mechanical and electrical performance at a cost low enough for mass application [22, 23]. Flexible coils have been used in imaging experiments where they have been wrapped round a former to increase the filling factor [24], and thin-film capacitors have been integrated to increase the Q-factor [25]. Tracking coils based on flexible substrates wrapped around catheters have also been proposed [26]. Plastic substrates have the potential for disposable use in procedures such as ERCP, the form factor needed for use in such a confined space and the flexibility needed to make the 90° turn used to exit the biopsy channel.

Recently [27], we demonstrated flexible resonant RF detectors combining electroplated Cu conductors with a substrate formed in the epoxy resist SU-8 [28]. Here, we describe two catheter detectors that combine a microfabricated coil with a cytology brush as shown in figure 2(*b*), and compare their performance. Type I coils use SU-8 as a substrate and have sufficiently limited flexibility that the coil must be mounted on a flat surface excised from the catheter. Type II coils use polyimide as a substrate and SU-8 as an interlayer and are flexible enough to wrap around the catheter. In section 2, we describe microfabrication. In section 3, we show

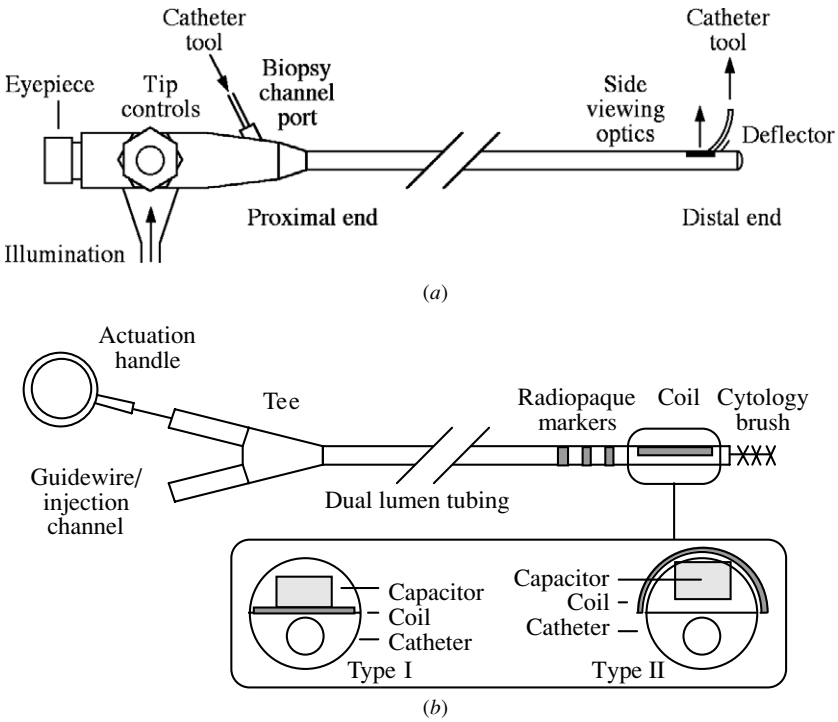

Figure 2. (*a*) Side viewing flexible endoscope used at ERCP; (*b*) cytology brush: general arrangement and integration of type I and II microcoils on the tip.

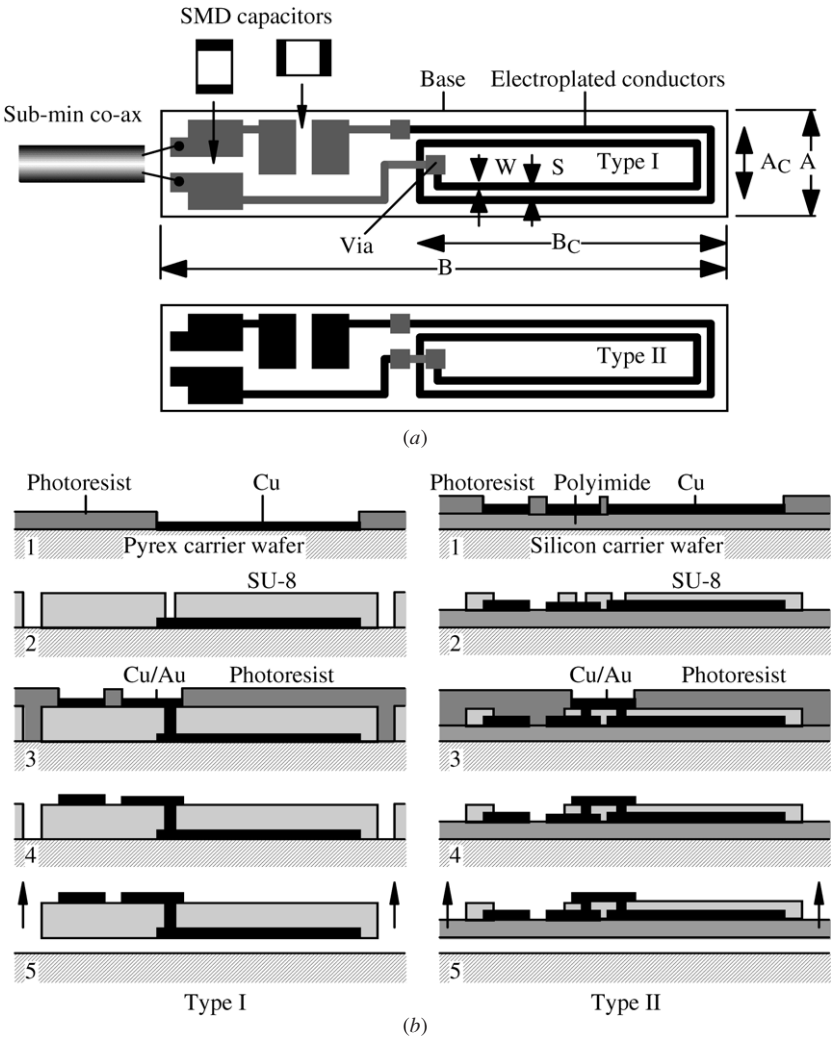

Figure 3. (*a*) Layout and (*b*) the fabrication process for type I and II microcoils.

that the coils have usable mechanical and electrical properties and demonstrate integration with a catheter. In section 4, we present the results of ^{1}H MRI using phantoms, which show a resolution of better than 1 mm at 1.5 T. Biliary imaging is demonstrated with *in vitro* porcine liver. Conclusions are presented in section 5.

2. Microcoil design and fabrication

In this section, we describe two different single-sided fabrication processes for microcoils on flexible plastic substrates.

2.1. Microcoil design

There are several difficulties in the fabrication of microcoils. To obtain sufficient electrical performance, thick multilayer conductors are needed. However, to pass the biopsy channel of an endoscope (3.2 mm ID), tuning and matching must be achieved with the minimum of additional components. Substrates that are stable enough for conductor formation and component attachment are therefore required. However, sufficient flexibility must be retained that the probe may be turned through 90° by a deflector for entry into the bile duct, without mechanical failure. The mechanical properties of SU-8 [28, 29] and the effect of process variations [30] have previously been characterized. We ourselves have found that SU-8 embrittles during processing. Here we show that flexible coils may be formed using thin layers of SU-8 with careful control of thermal load.

2.2. Microcoil fabrication

Microcoils were fabricated as rectangular spirals designed for use with their long axis parallel to a catheter, using the two layouts of figure 3(*a*). For type I coils, this arrangement provides a two-turn inductor on one side of an SU-8 substrate connected by vias to contact pads for a capacitor on the other. For type II coils, the inductor and pads were located on the same side of a polyimide substrate, and an electroplated bridge insulated by SU-8 used to connect to the inside of the inductor spiral. Coils were designed for integration on catheters with a diameter of 8 French (1 Fr = 1/3 mm). The substrate width of type I coils was therefore taken as $A = 2.7$ mm, and the coil width as $A_C = 2$ mm. Because of stress-induced bending of

the SU-8 substrates, only relatively short type I dies could be fabricated, so the overall die length was taken as $B = 25$ mm and the coil length as $B_C = 10$ mm. Wider substrates were required to wrap around the catheter, so the substrate width of type II coils was taken as $A = 7.5$ mm and the coil width as $A_C = 4.2$ mm. Longer type II dies could be fabricated, and coil lengths up to $B_C = 40$ mm in steps of 5 mm were used. In each case, the conductor width W and separation S were 200 μm and 100 μm.

Coils were fabricated using the two alternative planar batch processes shown in figure 3(*b*), which use many common process steps. In each case a 100 mm diameter wafer was used as a temporary carrier while patterning and electroplating were carried out on a plastic layer. Because of the intended application, non-magnetic materials were used throughout and common adhesion layers such as Cr and Ni were avoided. The plastic parts are then detached to provide a set of flexible substrates carrying an embedded RF electrical circuit.

For type I coils, the carrier was a Pyrex wafer. The spiral conductor tracks were formed first. The wafer was first cleaned using a Piranha etch followed by an oxygen plasma etch, and then sputter coated in a seed layer of 30 nm Ti and 200 nm Cu metal. A mould for electroplating was then formed using 20 μm of AZ 9260 photoresist, which was patterned using UV lithography. The seed layer was oxygen plasma cleaned, and 12 μm thickness of Cu was deposited by electroplating in Technic FB Bright Acid solution (Lektrachem Ltd, Nuneaton, UK) (step 1). The resist was then stripped in acetone, and the exposed seed layer removed by wet etching. The plastic structural layer was then formed. A 100 μm thick layer of SU-8 2025 epoxy resist (Microchem Corp., Newton, MA) was formed by spin coating over the coil windings, which left the conductors almost entirely buried in plastic. Processing was based on manufacturer's data [43]. Two spin-coating steps were used, and the exposure was split into two, to avoid overheating. After post-exposure baking, development was carried out in EC solvent, and finally the layer was hard baked (step 2). Vias, tracks and contact pads were then formed on the upper surface of the SU-8. The wafer was cleaned again, and coated with a further Ti/Cu seed layer. A second plating mould was formed using 20 μm of AZ 9260 resist. 12 μm of Cu was then electrodeposited as before. To protect the exposed contacts, 100 nm thickness of Au was deposited using ECF 60 solution (Metalor Technologies, Birmingham, UK) (step 3). The resist and seed layers were then stripped, and the wafer cleaned (Step 4). Coils were tested electrically and failed vias were repaired using silver-loaded epoxy (Epo-Tek H20E, Promatech, Cirencester, UK) before the coils were separated from the substrate by thermal shock—3 min heating at 200 °C (step 5).

For type II coils, a 25 μm thick polyimide sheet was stretched over a silicon wafer and anchored using Kapton tape. Cu conductors were then formed as above, by electroplating inside a mould (step 1). Care was required to prevent overheating of the film during RF sputtering, and adhesion of photoresist to the mask during lithography. A 2.5 μm thick layer of SU-8 was then deposited and patterned to act as a dielectric interlayer (step 2). An airbridge was then formed, by electroplating inside a further mould (step 3). The mould was removed and the exposed device surface was cleaned. The polyimide sheet was then detached from its carrier and individual coils were separated using a craft knife (step 5).

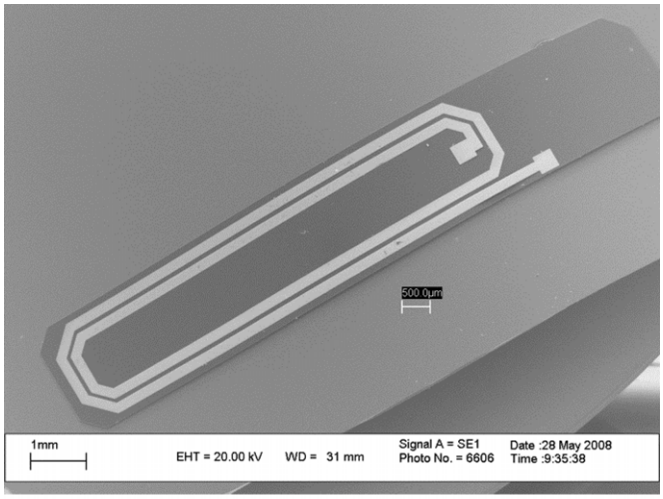

(*a*)

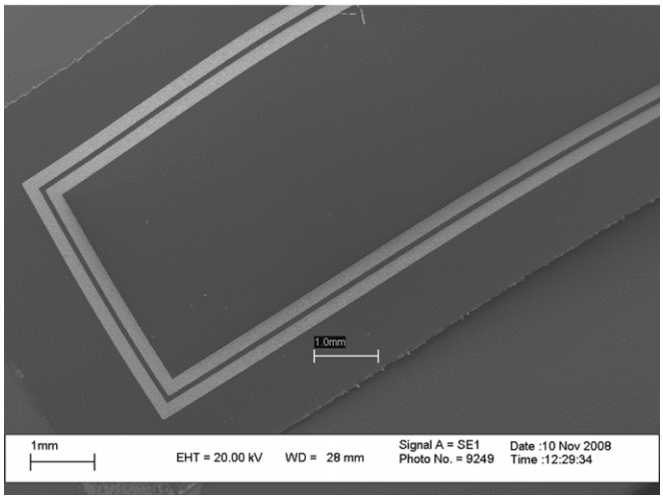

(*b*)

Figure 4. SEM views of (*a*) type I and (*b*) type II coils.

Figures 4 shows a scanning electron microscope view of a completed type I conductor spiral, showing how the conductors are entirely embedded in SU-8. Via pads lie at the upper RH end of the die, and connect to capacitor mounting pads on the far side. Figure 4(*b*) shows a SEM view of a type II inductor, showing the alternative arrangement of conductors on top of the polyimide layer. By comparison with the SU-8 substrate, the surface of the polyimide is relatively rough. Despite this, coils with comparable electrical performance were obtained.

3. Microcoil characterization and catheter assembly

In this section, we present the results of mechanical and electrical characterization of microcoils and describe their integration into a commercial cytology brush.

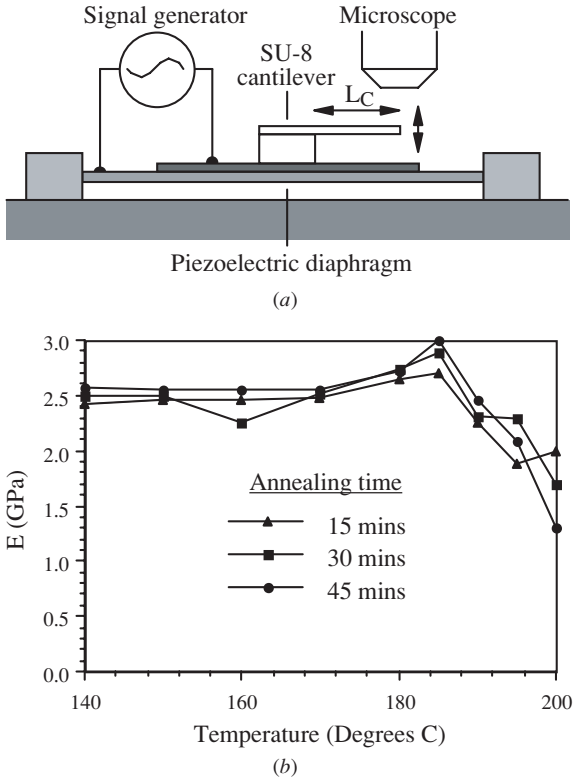

Figure 5. (*a*) Arrangement for mechanical characterization of SU-8; (*b*) variation of Young's modulus of SU-8 with annealing temperature, for different annealing times.

3.1. Mechanical characterization

SU-8 adheres well to many materials. However, since it has a high coefficient of thermal expansion (52×10^{-6} [28]) it can be detached from a low expansion substrate by thermal shock. Because elevated temperatures degrade SU-8, the effect of temperature was investigated by measuring Young's modulus after annealing a batch of bare SU-8 dies. Their depth d, width w and overall length were first measured, and their density found using a microbalance as $\rho \approx 1060$ kg m^{-3}. The dies were then arranged as suspended cantilevers on a piezoelectric diaphragm as shown in figure 5(*a*), using a travelling microscope to determine the overhang L_C. The diaphragm was driven from a sinusoidal signal generator, and the resonant frequency f_r of the cantilever was found. Typically, $f_1 \approx 150$ Hz for $L_C \approx 10$ mm and $d \approx 80$ μm. Young's modulus E was then extracted from the standard formula for the lowest order resonance of a cantilever, ${\omega_1}^2 = (\beta^2/{L_C}^2)\sqrt{(EI/\rho A)}$, where $\omega_1 = 2\pi f_1$, $\beta = 3.52$, $I = wd^3/12$ is the second moment and $A = wd$ is the cross-sectional area [31].

Figure 5(*b*) shows the temperature variation of Young's modulus, for different annealing times. For low temperatures, E is approximately constant at 2.5 GPa, in agreement with manufacturer's data (2.0 GPa). However, variations start to occur above 170 °C, with E first rising to a peak and then falling as the glass transition temperature T_g (210 °C) is approached. These results show clearly that the peak process temperature should be kept below T_g, and that the time spent at high process temperatures should be minimized.

Experiments carried out to detach type I dies from Pyrex carriers in liquid N_2 were unsuccessful. Thermal detachment was therefore performed at a high temperature—3 min heating at 200 °C. The mechanical behaviour of released dies was then consistent. The dies had small out-of-plane curvature, but could be flexed without breaking or detaching embedded conductors. However, raised contact pads were prone to detachment. Small (<1 mm) bending radii R resulted in brittle failure. At this point the maximum tensile strain is $\varepsilon_{max} = d/2R = 5 \times 10^{-2}$, in agreement with manufacturer's data ($\varepsilon_b = 6.5 \times 10^{-2}$). Failure typically occurred at via holes, due to stress concentrations. These results imply that tighter bending could be achieved using thinner SU-8 layers. However, use of such thin structures requires the support of a catheter. In contrast, type II dies could be bent repetitively without degradation, and wrapped around catheters down to 6 Fr diameter.

3.2. Catheter probe

Catheter probes were constructed from 8 Fr Cytomax II biliary cytology brush units (Cook Medical, Limerick, RoI). The unit has the arrangement shown in figure 2(*b*), and is formed from ≈2 m of dual lumen PTFE tubing, which provides one channel for a brush actuation wire and a second for a guidewire or for contrast agent injection. X-ray markers are located near the tip. To integrate a microcoil, all magnetic parts (the brush, and a Luer syringe fitting on the contrast injection channel) were first removed. A short length of tubing with a D-shaped section containing the guidewire channel was removed using a scalpel. Type I coils were attached to the resulting planar surface using heat-shrink bands. Type II coils were wrapped around the catheter, and attached using heat shrink with the capacitors located in the excised region. Electrical connection between the coil and a length of 0.8 mm diameter non-magnetic 50 Ω Bluetooth co-axial cable (Axon Cable, Dunfermline, UK) in the guidewire channel was made using conducting epoxy (Epo-Tek H20E). Figures 6(*a*) and (*b*) show close-up views of catheter ips containing type I and II coils, respectively.

3.3. Electrical characterization

Protons have spin 1/2 and two spin states with an energy difference $\Delta E = \gamma h B_0/2\pi$. Here γ is the gyromagnetic ratio, h is Planck's constant and B_0 is the magnetic flux. If this energy is detected by near-field Faraday induction, the frequency is $f = \gamma B/2\pi$. For protons, $\gamma = 2.675 \times 10^8$ rad s^{-1} T^{-1}, so the frequency scales with field at 42.57 MHz T^{-1} [32]. In a 1.5 T system (commonly used for human imaging), $f =$ 63.8 MHz. Non-magnetic 0805 surface mount capacitors (SRT Micro Céramique, Vendome, France) were used to achieve resonance at 63.8 MHz and match impedance to 50 Ω, using an Agilent E5061 A network analyser. For type I coils, tuning and matching were carried out before integration on the catheter. For type II coils, whose inductances alter as they are wrapped round the catheter, tuning and matching were carried out after

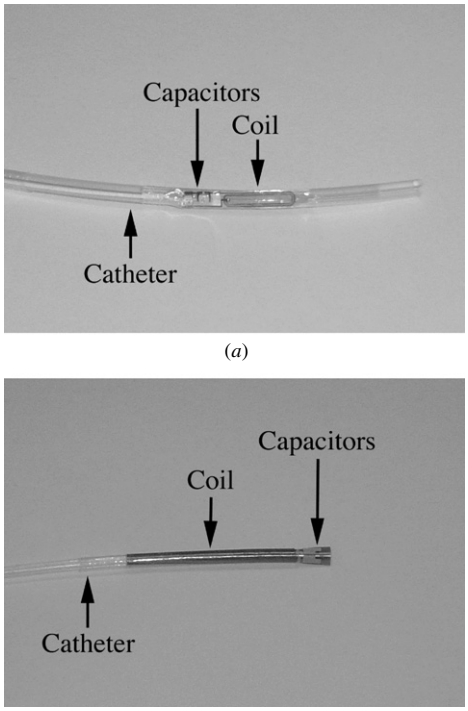

Figure 6. Cytology brush unit, after integration of (*a*) type I and (*b*) type II microcoils.

integration. The capacitance values used are given in table 1, together with other electrical performance parameters.

Table 1. Electrical parameters for type I and II microcoils.

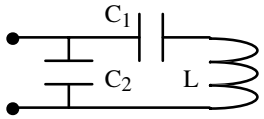

Microcoil	Length (mm)	L (nH)	C_1 (pF)	C_2 (pF)	Unloaded Q
Type I	10	46	220	330	19
Type II	35	190	39	144	16

Figures 7(*a*) and (*b*) show the frequency variation of impedance of type I and type II coils, respectively. The resonant frequencies are almost identical, and there are only small variations in impedance, showing that similar performance has been achieved despite large constructional differences. Type I coils had unloaded Q-factors of ≈20; Type II coils had slightly lower Q-factors. Figures 7(*c*) and (*d*) show the frequency variation of S_{21} obtained by inductive excitation of the catheter coil. Type II coils are more sensitive to overall signal, by virtue of their increased length. These figures also show the frequency variation of S_{11} for type I and II coils, respectively. In each case, the coil is well matched. After verification of electrical functionality, the assembly was sealed in heat-shrink tubing. Because type I coils present a discontinuous surface with protruding capacitors, sealing was ineffective, and leaks were observed during immersion tests. In contrast, type II coils could be sealed well enough to operate immersed in water for extended periods.

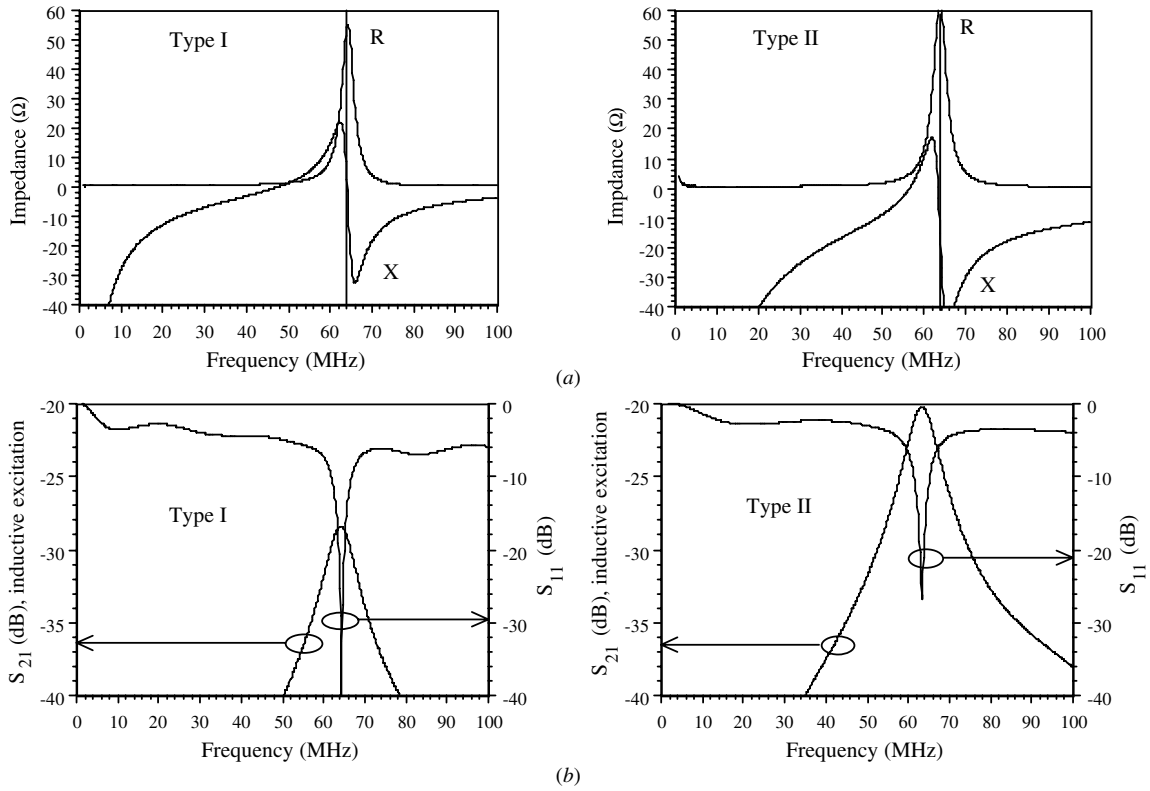

Figure 7. Frequency variations of (*a*) impedance and (*b*) scattering parameters of type I and II microcoils.

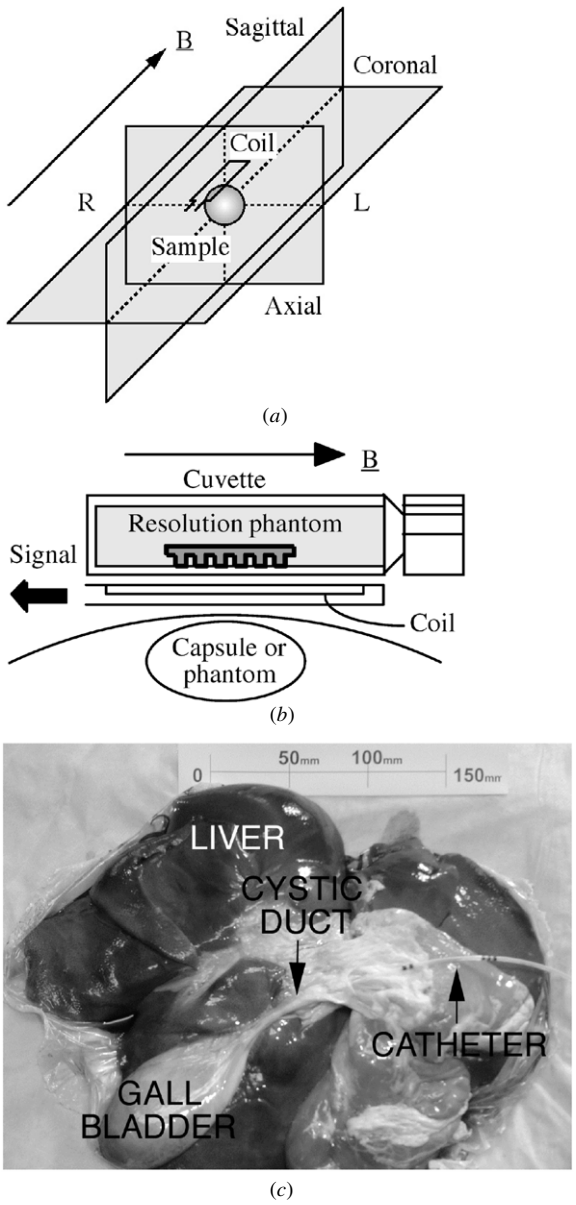

Figure 8. (*a*) Orientation of microcoil in scanner; (*b*) arrangement for phantom imaging and (*c*) arrangement for biliary imaging.

4. Magnetic resonance imaging

In this section, we present the results of ^{1}H magnetic resonance imaging experiments aimed at establishing the resolution of the catheter probe using phantoms and *in vitro* tissue.

4.1. Magnetic resonance imaging

^{1}H MRI was performed using a 1.5 T GE HD Signa Excite scanner at St Mary's Hospital, Paddington, London, UK. The system body coil was used for transmission and the microcoil was connected to the auxiliary coil input for reception. Initial experiments were performed with a bare microcoil, which was placed at the isocentre in the coronal plane as shown in figure 8(*a*). In each case, the microil was first autotuned using a large spherical phantom, using a fast recovery fast spin echo (FRFSE) sequence, and the transmission gain was gradually increased to the maximum allowed by the system. A number of experiments were then carried out, using the sequence parameters in table 2.

Table 2. Imaging parameters for the different magnetic resonance imaging experiments.

Experiment	1	2	3
Microcoil	Type I	Type II	Type II
Object	Bar phantom	Bolt phantom	Liver
Sequence	T_2-weighted 3D GRE FRFSE	T_2-weighted 3D GRE FRFSE	T_1-weighted 2D SE
TR (msec)	33	33	400
TE (msec)	15	15	12
Flip angle (°)	10	10	90
No of slices	28	28	18
Slice thickness (mm)	1.2	1.2	3
FOV (mm)	80 × 40	80 × 40	80 × 80
Pixels in slice	192 × 160	256 × 224	192 × 160
NEX	4	6	2
Acquisition time	5 min 42 s	11 min 53 s	4 min 19 s

SE: spin echo; GRE: gradient echo; FRFSE: fast recovery fast spin echo.

4.2. Resolution tests—type I microcoils

Resolution tests were first carried out with type I coils (experiment 1). A combination of a cod-liver-oil capsule measuring 10 mm dia × 15 mm and a glass cuvette containing a microfabricated phantom in solution was used as a sample, to demonstrate the sensitive range and the resolution. The phantom was a moulded plastic structure containing 1 mm bars separated by 1 mm gaps. The microcoil was placed between the capsule and the phantom as shown in figure 8(*b*), and localizer scans were used to centre the image. Imaging was carried out using a relaxation recovery time (TR) of 33 ms and an echo time (TE) of 15 ms. Images were acquired using a T_2-weighted FRFSE sequence which recovered 28 slices of 1.2 mm thickness, with 192 × 160 pixels per slice in an 80 mm × 40 mm field of view (FOV). To improve image signal-to-noise ratio each step of the acquisition was repeated. The number of such excitations (NEX) was 4, and the acquisition time was 5 min 42 s. Figure 9(*a*) shows a sagittal MR image of the experimental arrangement in figure 8(*c*). Here the image is rotated by 90°, but the cod-liver-oil capsule and the cuvette are both visible, and the resolution phantom can been seen at the base of the cuvette. Some distortion may be seen at the bottom left of the capsule, which may be due to artefacts. However, figure 9(*b*) shows a coronal image, in which the bar pattern is clearly resolved.

4.3. Resolution tests—type II microcoils

The resolution tests were repeated using type II coils (experiment 2). Because of their larger sensitive length, the resolution phantom was replaced with an M4 nylon nut and cheesehead bolt in solution and the capsule with

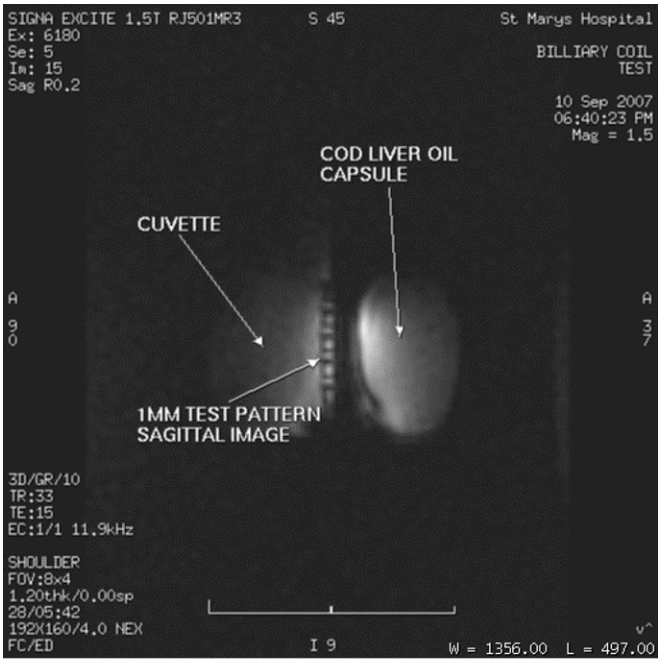

(*a*)

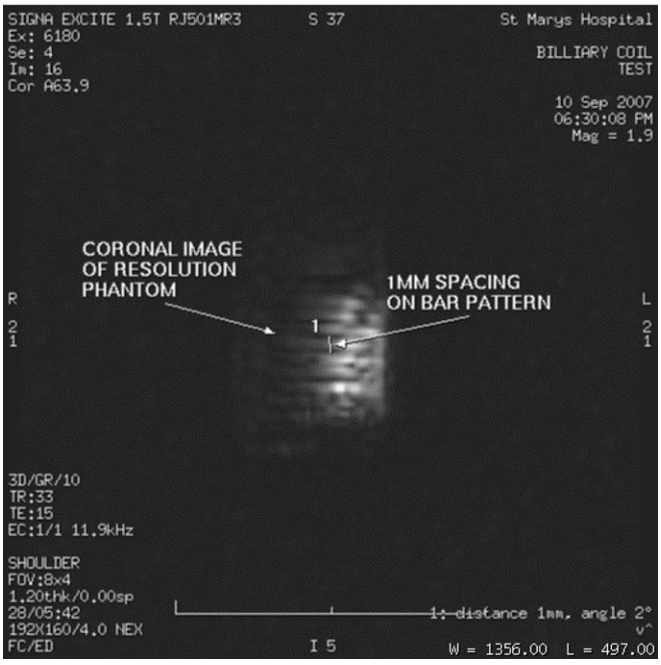

(*b*)

Figure 9. ^{1}H MR images obtained using a type I coil of a resolution test phantom in (*a*) sagittal and (*b*) coronal planes in experiment 1.

a large spherical phantom. Since the M4 tooth pitch (0.7 mm) was expected to place severe demands on resolution capability, the number of pixels per slice was increased to 256 × 224 and the number of excitations to 6. These changes approximately doubled the acquisition time, to 11 min 53 s. However, figure 10(*a*) shows a sagittal image, in which the shank, head, screwdriver slot and individual teeth of the bolt are clearly visible, demonstrating strongly sub-millimetre imaging.

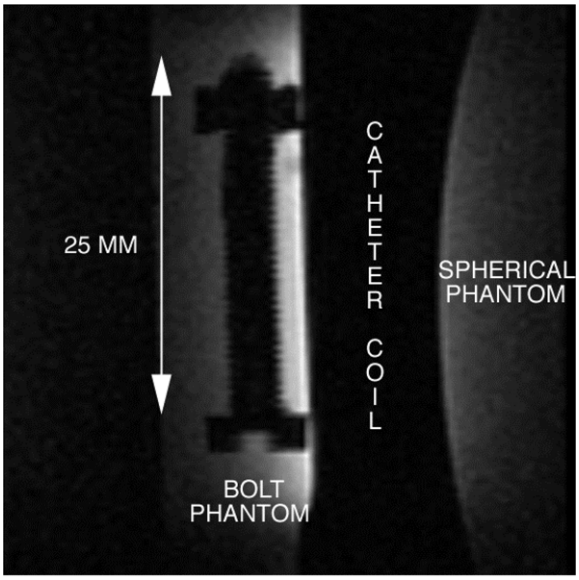

(*a*)

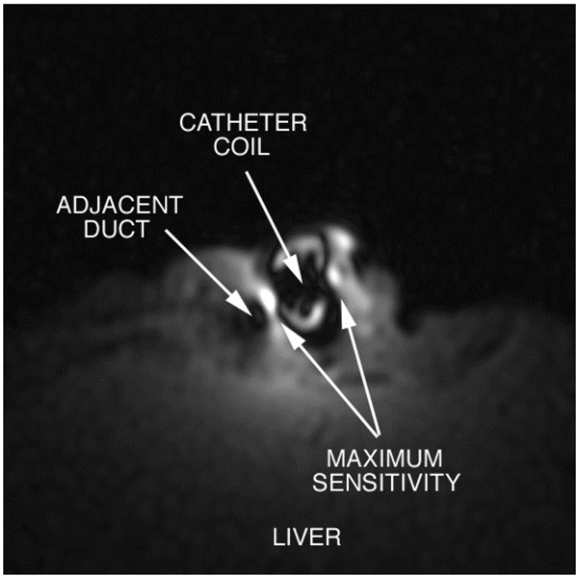

(*b*)

Figure 10. ^{1}H MR images obtained using a type II coil of (*a*) a resolution test phantom in the sagittal plane in experiment 2 and (*b*) porcine liver in the axial plane in experiment 3.

4.4. In vitro imaging tests—type II microcoils

In vitro biliary imaging was then demonstrated using type II coils (experiment 3). A whole porcine liver with attached gall bladder and biliary tree was arranged in a bowl with the ducts again at the isocentre and parallel to the magnet bore. A catheter coil was then inserted into the cystic duct via an incision as shown in figure 8(*c*). Liver tissue has a less than ideal MR response, as it has a short spin–spin relaxation time T_2. Images were therefore acquired using a T_1-weighted 2D spin echo sequence with TR = 400 ms and TE = 12 ms, 18 slices of 3 mm thickness, 192 × 160 pixels per slice, 80 mm × 80 FOV and NEX = 2. Images revealing anatomical detail were obtained to a depth >1.5 cm, 360° around the coil and along 3.2 cm of its length. Figure 10(*b*) shows an axial image

in which bile ducts and blood vessels can be distinguished. The conductors are indicated by the two bright spots of maximum sensitivity on either side of a dark circle containing the catheter.

These initial results demonstrate that microcoils can provide useful imaging performance. However, improvements are required to characterize and remove artefacts. Increases in SNR are also required, since the images shown here require acquisition times beyond the limit of breath holding. As a result, *in vivo* use is likely to require motion correction.

5. Conclusions

We have demonstrated two single-sided wafer-scale batch fabrication processes for flexible planar microcoils for signal reception in magnetic resonance imaging, based on electroplated conductors and plastic substrates. The first uses SU-8 substrates and the second polyimide substrates and SU-8 interlayers. Each can yield freestanding microcoils with spiral windings. However, careful control of temperatures used in SU-8 processing is required to retain flexibility, and improved mechanical performance is obtained using polyimide substrates and thin SU-8 layers. When combined with surface mount capacitors, the assembly can be integrated on the tip of a catheter probe designed to pass the biopsy channel of a duodenoscope in endoscopic retrograde cholangiopancreatography. Mechanical performance is adequate, electrical performance is repeatable, and ^{1}H MRI with sub-millimetre resolution has been demonstrated at 1.5 T. Further reliability qualification is required before any clinical evaluation. Replacement of magnetic components in all of the catheter-based tools used during ERCP with non-magnetic equivalents, construction of a non-magnetic endoscope, and hardware and software for motion compensation during *in vivo* imaging is also needed. This work is in progress.

Acknowledgments

The authors are grateful to EPSRC for financial support, under Grant EP/E005888/1 '*In vivo* biliary imaging and tissue sampling', and to Dr Rob Dickinson, Dr Shakil Awan, Dr Shahid Khan and Professor Mark Thursz for very helpful discussions. SDT-R, CAW and WMWG are grateful to the NIMR Biomedical Research Facility for infrastructure support.

References

[1] Khan S A, Thomas H C, Davidson B R and Taylor-Robinson S D 2005 Cholangio-carcinoma *Lancet* **366** 1303–14

[2] Taylor-Robinson S D, Toledano M B, Arora S, Keegan T J, Hargreaves S, Beck A, Khan S A, Elliott P and Thomas H C 2001 Increase in mortality rates from intrahepatic cholangiocarcinoma in England and Wales 1968–1998 *Gut* **48** 816–20

[3] Vennes J A, Jaconson J R and Silvis S E 1973 Endoscopic cholangiography in the diagnosis of obstructive jaundice *Gastroenterology* **64** A132/815

[4] Foutch P G, Kerr D M, Harlan J R, Manne R K, Kummet T D and Sanowski R A 1990 Endoscopic retrograde wire-guided brush cytology for diagnosis of patients with malignant obstruction of the bile duct *Am. J. Gastroenterol.* **85** 791–5

[5] Kantor H L, Briggs R W and Balaban R S 1984 *In vivo* ^{31}P nuclear magnetic resonance measurements in canine heart using a catheter-coil *Circ. Res.* **55** 261–6

[6] Hurst G C, Hua J, Duerk J L and Cohen A M 1992 Intravascular (catheter) NMR receiver probe: preliminary design analysis and application to canine iliofemoral imaging *Magn. Reson. Med.* **24** 343–57

[7] Quick H H, Ladd M E, Zimmermann-Paul G G, Erhart P, Hofmann E, von Schulthess G K and Debatin J F 1999 Single-loop coil concepts for intravascular magnetic resonance imaging *Magn. Reson. Med.* **41** 751–8

[8] Crottet D, Menli R, Wicky S and van der Kink J J 2002 Reciprocity and sensitivity of opposed-solenoid endovascular MRI probes *J. Magn. Reson.* **159** 219–25

[9] Dumoulin C L, Souza S P and Darrow R D 1993 Real-time position monitoring of invasive devices using magnetic resonance *Magn. Reson. Med.* **29** 411–5

[10] Burl M, Coutts G A, Herlihy D, Hill-Cottingham R, Eastham J E, Hajnal J V and Young I R 1999 Twisted-pair RF coil suitable for locating the track of a catheter *Magn. Reson. Med.* **41** 636–8

[11] Zhang Q, Wendt M, Aschoff A J, Lewin J S and Duerk J L 2001 A multielement RF coil for MRI guidance of interventional devices *J. Magn. Reson. Imaging* **14** 56–62

[12] Zuehlsdorff S, Umathum R, Volz S, Hallscheidt P, Fink C, Semmler W and Bock M 2004 MR coil design for simultaneous tip tracking and curvature delineation of a catheter *Magn. Reson. Med.* **52** 214–8

[13] Weiss C R, Georgiades C, Hofmann L V, Schulick R, Choti M, Thulavath P, Bluemke D A and Arepally A 2006 Intrabiliary MR imaging: assessment of biliary obstruction with the use of an intraluminal MR receiver coil *J. Vasc. Interv. Radiol.* **17** 845–53

[14] Ocali O and Atalar E 1997 Intravascular magnetic resonance imaging using a loopless catheter antenna *Magn. Reson. Med.* **37** 112–8

[15] Peck T L, Magin R L, Kruse J and Feng M 1994 NMR microspectroscopy on 100-mm planar RF coils fabricated on gallium arsenide substrates *IEEE T. Biomed. Eng.* **41** 706–9

[16] Stocker J E, Peck T L, Webb A G, Feng M and Magin R L 1997 Nanoliter volume, high-resolution NMR microspectroscopy using a 60-mm planar microcoil *IEEE T. Biomed. Eng.* **44** 1122–7

[17] Neagu C R, Jansen H V, Smith A, Gardeniers J G E and Elwenspoek M C 1997 Characterization of a planar microcoil for implantable microsystems *Sensors Actuators* A **62** 599–611

[18] Renaud L, Armenean M, Berry L, Kleimann P, Morin P, Pitaval M, O'Brien J, Brunet M and Saint-Jalmes H 2002 Implantable planar rf microcoils for NMR microspectroscopy *Sensors Actuators* A **99** 244–8

[19] Syms R R A, Ahmad M M, Young I R, Gilderdale D J and Collins D J 2006 Microengineered needle micro-coils for magnetic resonance spectroscopy *J. Micromech. Microeng.* **16** 2755–64

[20] Dechow J, Forchel A, Lanz T and Haase A 2000 Fabrication of NMR-microsensors for nanoliter sample volumes *Microelectr. Eng.* **53** 517–19

[21] Massin C, Boero C, Vincent F, Abenhaim J, Besse P A and Popovic R S 2002 High-Q factor RF planar microcoils for micro-scale NMR spectroscopy *Sensors Actuators* A **97–8** 280–8

[22] Coutrot A-L, Dufour-Gergam E, Quemper J-M, Martincic E, Gilles J-P, Grandchamp J P, Matlosz M, Sanchez A,

Darasse L and Ginefri J-C 2002 Copper micromolding process for NMR microinductors realisation *Sensors Actuators* A **99** 49–54

[23] Woytasik M, Dufour-Gergam E, Grandchamp J-P, Martincic E, Poirer-Quinot M, Ginefri J-C, Darasse L and Vautier J 2004 Copper microcoils dedicated to NMR imaging *Proc. MME'04 (Leuven, Belgium, Sept. 5–7)* pp 143–6

[24] Woytaskik M *et al* 2007 Characterisation of flexible RF microcoils dedicated to local MRI *Microsyst. Technol.* **13** 1575–80

[25] Ellersiek D, Harms S, Casanova F, Blümich B, Mokwa W and Schnakenberg U 2005 Flexible RF microcoils with integrated capacitor for NMR applications *Proc. MME'05 (Göteborg, Sweden, Sept. 4–6)* pp 256–9

[26] Uelzen T h, Fandrey S and Müller J 2006 Mechanical and electrical properties of electroplated copper for MR-imaging coils *Microsyst. Technol.* **12** 343–51

[27] Ahmad M M, Casperz W, Young I R, Taylor-Robinson S, Syms R R A and Gedroyc W 2008 Flexible microcoils for *in-vivo* biliary imaging *Proc. 19th Micromechanics Europe Workshop (Aachen, Germany, Sept 28–30)* pp 275–8

[28] SU8 2000 Permanent epoxy negative photoresist. Processing guidelines for SU-8 2100 and SU-8 2150 http://www.microchem.com

[29] Lorenz H, Despont M, Fahrni N, LaBianca N, Renaud P and Vettinger P 1997 SU-8: a low-cost negative resist for MEMS *J. Micromech. Microeng.* **7** 121–4

[30] Sameoto D, Tsang S-H, Foulds I G, Lee S W and Parameswaram M 2007 Control of the out-of-plane curvature in SU-8 compliant microstructures by exposure dose and baking times *J. Micromech. Microeng.* **17** 1093–98

[31] Thomson W T 1993 *Theory of Vibration with Applications* 4th edn (London: Chapman and Hall)

[32] Morris P G 1986 *Nuclear Magnetic Resonance Imaging in Medicine and Biology* (Oxford: Clarendon Press) chapter 5